SEM/X-RAY IMAGING OF CEMENT-BASED MATERIALS

Bentz, D.P. and Stutzman, P.E.
National Institute of Standards and Technology, Gaithersburg, MD USA
Haecker, C.J.
Wilhelm Dyckerhoff Institut, Wiesbaden, GERMANY
Remond, S.
Centre Scientifique et Technique du Batiment, FRANCE

Abstract

Scanning electron microscopy and X-ray imaging techniques have been developed for imaging the complex microstructure of cement-based materials such as cement powder and fly ash. By combining the information available in the backscattered electron and relevant X-ray images, an accurate segmentation of the image into individual cement clinker phases or other components can be accomplished. This paper reviews the image acquisition and processing techniques used in performing this analysis, as well as the statistics that can be used to characterize the final 2-D microstructures, such as area fractions, surface fractions, and two-point correlation functions. In addition, two applications are presented: 1) the imaging of a series of fly ashes from different sources, and 2) the analysis of cement microstructure as a function of grinding fineness. The resultant images provide the quantitative characterization needed for input into three-dimensional computer models of cement hydration and microstructural development.

1 Introduction

Cementitious materials are inherently complex from a microstructural viewpoint. The starting cement powder is a multi-size, multi-phase particulate system whose chemical and physical properties control the hydration behavior of the cement paste. While this paper focuses on the microstructure of these materials at the scale of micrometers, it should be noted that such complexity exists at scales ranging from nanometers (the gel structure of the calcium silicate hydrate) to millimeters (the scale of aggregates in the concrete), requiring the application of a multi-scale approach to the microstructural modelling of concrete materials [1].

Scanning electron microscopy is a powerful technique for analyzing cement-based materials [2], and has been applied successfully to cement clinkers [3], cement powders [4, 5], and hydrated cement pastes and concretes [6]. The SEM provides high contrast images that can be segmented to identify the component phases comprising the complex cement microstructure. In this paper, the image acquisition and processing techniques used in this process are outlined, spatial statistics that can be used to characterize the 2-D (and 3-D) microstructure are enumerated, and example results for the imaging of both fly ashes and cement powders are presented.

Microscopy Applied to Building Materials, 7th Euroseminar. Proceedings. June 29-July 2, 1999, Delft,The Netherlands, Delft University of Technology, Delft,The Netherlands, Pietersen, H. S.; Larbi, J. A.; Janssen, H. H. A., Editors, 457-466 pp, 1999.

2 Sample Preparation and Imaging Techniques

2.1 Sample Preparation

The sample preparation techniques have been described in detail elsewhere [4], but will be briefly presented here. To prepare a polished specimen for viewing in the SEM, approximately 25 grams of the powder to be imaged is blended with an epoxy resin to form an extremely viscous paste. The resin/powder mixture is pressed into a mold and cured at 60 °C for 24 hours. The cured specimen is then cut to obtain a plane surface for imaging.

Saw marks are removed by grinding with 400 grit followed by 600 grit sandpaper. Final polishing is done on a lap wheel with (6, 3, 1, and 0.25) μm diamond paste for 30 seconds each. After each polishing, the specimen is cleaned using a clean cloth and after the final polishing step, ethanol is used to remove any residual polishing compound. The final polished specimen is coated with carbon to provide a conductive surface for viewing in the SEM.

2.2 Image Acquisition

The specimen is placed in the SEM viewing chamber, and signals are collected for the backscattered electrons and X-rays. Typical accelerating voltage and probe current for the backscattered electron images are 12 kV and 2 nA, respectively. For the X-ray images, the probe current is increased to about 10 nA. For cements, in addition to the backscattered electron signal, X-ray images are collected for Ca, Si, Al, Fe, S, K, and Mg. For fly ash, other X-ray signals may be desirable such as Cl, Zn, or Pb. Because these X-ray images are collected at the same location as the backscattered electron image, this series of images can be combined to determine the mineral phase present at each location (pixel) in the two-dimensional image (typically 512 pixels by 400 pixels in size). Typically, magnifications of 250X or 500X are employed for obtaining the SEM images.

2.3 Image Processing

To process the input SEM/X-ray images and determine the distribution of phases, a decision tree is traversed for each pixel location in the images. Example decision trees for a typical cement powder and a fly ash containing substantial chloride are shown in Figures 1 and 2, respectively. In these figures, X^* represents a critical threshold greylevel value, pixels having a greylevel greater than the value of X^* being considered to contain the element of interest and those with a greylevel below X^* being classified as not containing the element. To determine the values of X^* for each element, the corresponding greylevel histogram [7] for each X-ray image is viewed. The greylevel histogram is a plot of the fraction of pixels containing each greylevel value (e.g., 0 to 255). For example, Figure 3 shows the greylevel histogram for the calcium signal image for a portland cement. The local minimum value between the two peaks would serve as a good estimate of Ca^* for this particular image. For some of the elements, the greylevel histogram contains only one peak and the analyst must estimate the appropriate value of X^* from the shoulder present on the right side of the peak. In all cases, the raw X-ray image can also be thresholded at different greylevel values, to produce a binary image that should represent the locations of each element in the 2-D image. If this value is set too low, many small isolated regions of element X (basically random noise) will appear. If this value is set too high, very little of element X will be present. Many modern image processing systems allow this threshold to be changed dynamically using a mouse or dial so that the analyst may quickly determine the "best" threshold value for a particular element.

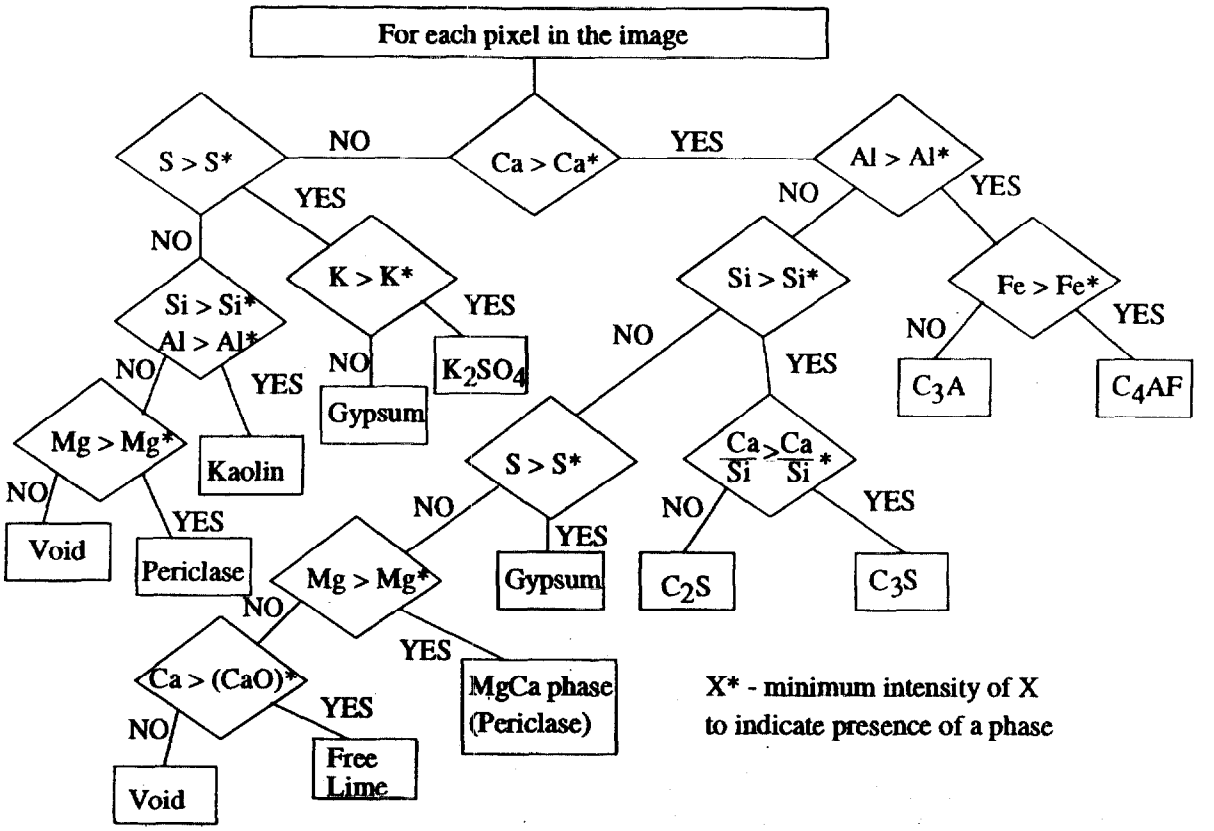

Figure 1: Segmentation algorithm for separating portland cement into its components. C_3S denotes tricalcium silicate, C_2S denotes dicalcium silicate, C_3A denotes tricalcium aluminate, C_4AF denotes tetracalcium aluminoferrite, and CaO corresponds to free lime.

After the segmentation tree is traversed, the segmented image produced will still contain a substantial amount of random noise. To improve the image quality, three "filters" are applied in succession to the processed image. First, all isolated one pixel "solid" pixels are converted to porosity. Second, all isolated one pixel "pores" (totally surrounded by solids) are converted to the majority surrounding solid phase. Finally, a median filter is applied to replace each solid pixel by the majority solid phase present in the surrounding neighborhood, typically 5 pixels × 5 pixels. This three-fold process removes the remaining noise present in the segmented image, producing an image ready for quantitative stereological analysis.

2.4 Stereological Parameters

The final processed image can be analyzed to determine any number of stereological parameters. For cement hydration, parameters of interest include phase area fractions and phase surface perimeter fractions. For an isotropic system, the area fraction of a phase present in a 2-D image will directly correspond to its volume fraction in three dimensions. Similarly, a phase's share of the total perimeter (solid pixels in contact with porosity) will correspond to its share of the total surface area in 3-D. The surface area fractions of the phases are particularly important for cement hydration as the hydration reactions with water occur at the surfaces of the particles.

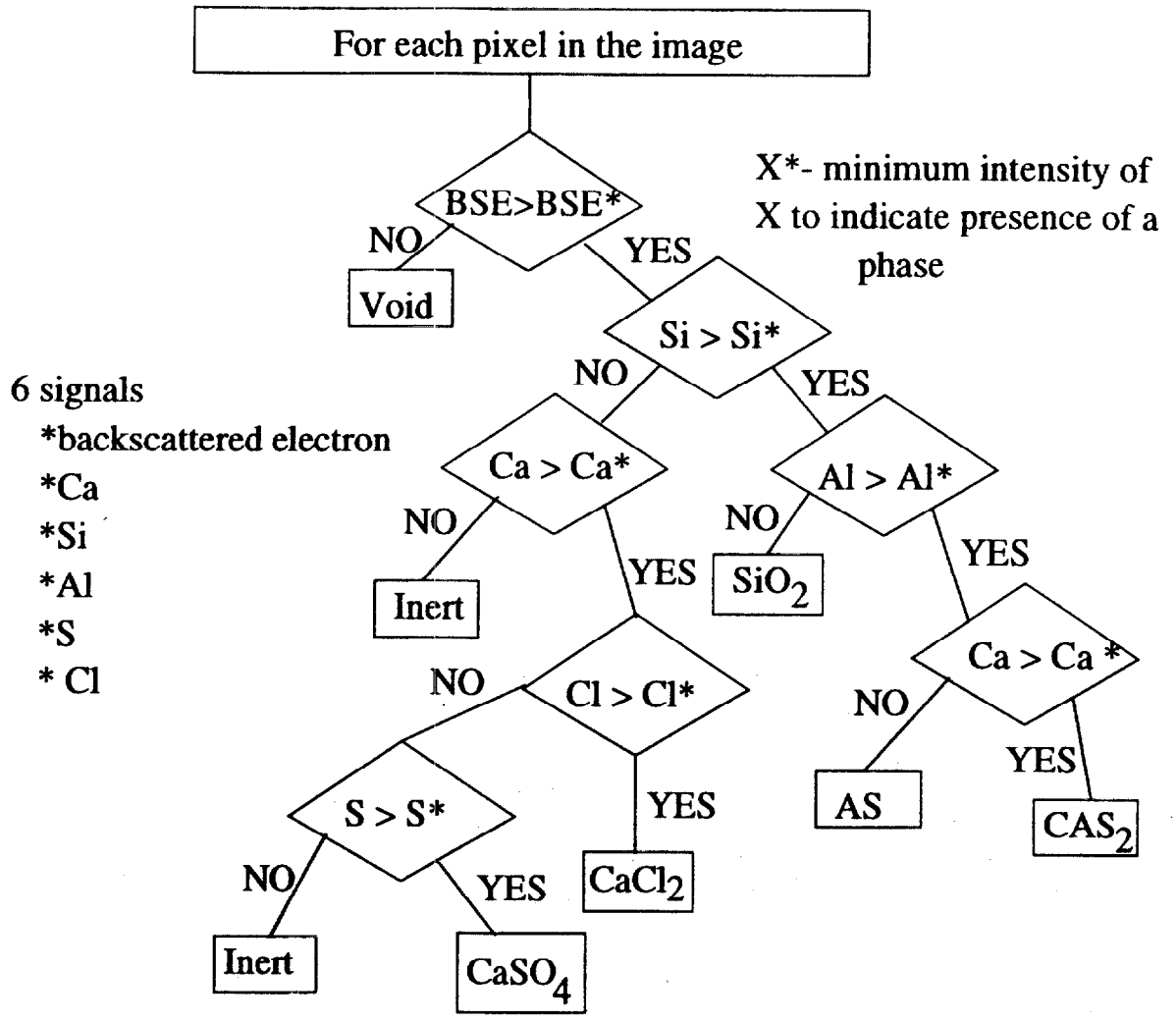

Figure 2: Segmentation algorithm for separating a municipal waste fly ash into its components. AS denotes an aluminosilicate phase and CAS_2 denotes calcium alumino-disilicate.

For an isotropic material, the spatial correlation functions are identical in two and three dimensions, simply being a function of distance, r. Thus, the measured 2-D correlation function for a phase or a combination of phases can be used to reconstruct a 3-D representation of the cement particles [8]. For an $M \times N$ image, the two-point correlation function for a phase, $S(x, y)$, is determined as:

$$S(x,y) = \sum_{i=1}^{M-x} \sum_{j=1}^{N-y} \frac{I(i,j) \times I(i+x, y+j)}{(M-x) \times (N-y)} \tag{1}$$

where I(x,y) is one if the pixel at location (x,y) contains the phase(s) of interest and 0 otherwise. S(x,y) is easily converted to S($r = \sqrt{x^2 + y^2}$) for distances r in pixels. Because the correlation function implicitly contains information on the volume fraction and specific surface of the phase(s) being analyzed, this function can be employed to reconstruct a three-dimensional representation of the cementitious particles that matches the phase volume and surface area fractions and correlation structure of the 2-D final SEM image. These starting

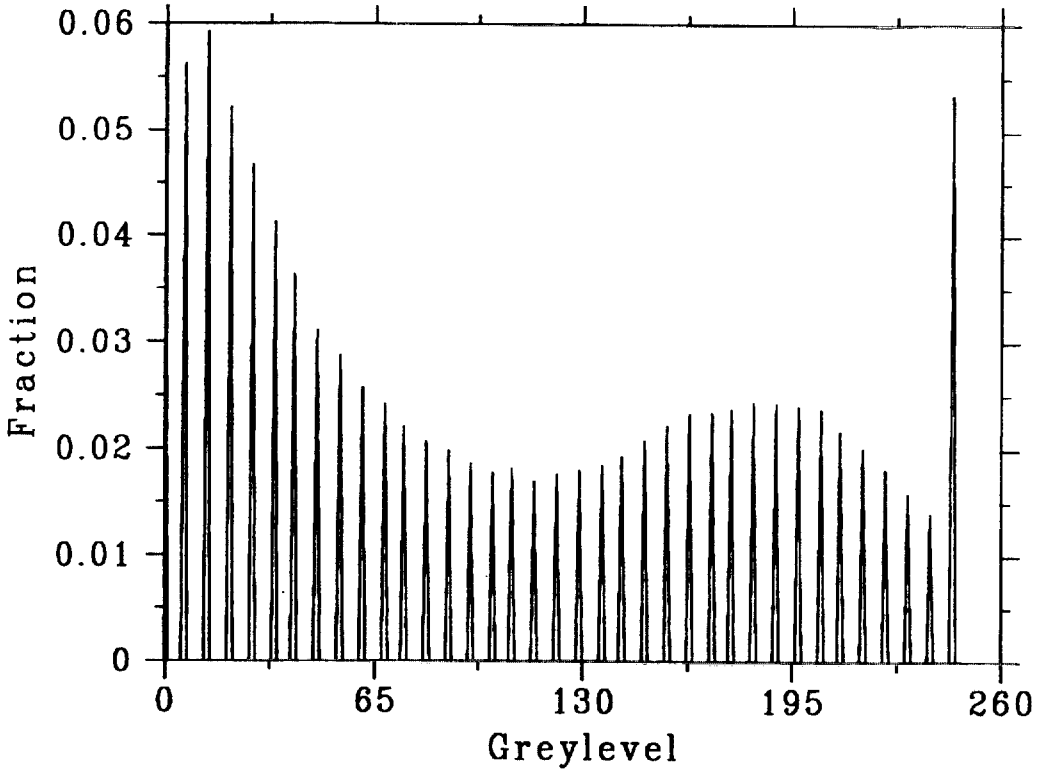

Figure 3: Greylevel histogram for calcium X-ray image for an ordinary portland cement.

3-D structures of cement particles in water, for example, are needed to provide accurate input for three-dimensional cement hydration and microstructural development computer models which predict the development of microstructure and properties of hydrating cement paste with time [8].

3 Results for Example Applications

3.1 Analysis of fly ashes

The above techniques have been applied to analyzing a variety of fly ashes [9]. Figures 4 and 5 contrast the appearance of a class F fly ash with that of one obtained from the incineration of a municipal waste. For the class F fly ash, the majority of the particles are spherical and monophase. Some hollow cenospheres can be observed as two-dimensional "rings" in the final processed image. For the municipal waste fly ash image, by contrast, the particles are irregularly shaped and tend to be multi-phase in nature. For this particular waste fly ash, a high concentration of calcium chloride is observed in the SEM/X-ray images, as indicated by strong signals for Ca and Cl in the corresponding X-ray images. Images such as these allow for a quantitative characterization of the fly ash with respect to phase volume fraction, phase surface area fractions, and phase distributions within the larger multi-phase particles. This quantitative analysis can then be used as input for cement hydration and microstructural models which include the reactions between the fly ash and the portland cement phases [9]. Thus, these images are critically needed for predicting the influence of a fly ash on the hydration chemistry, microstructure development, and properties of a cementitious system.

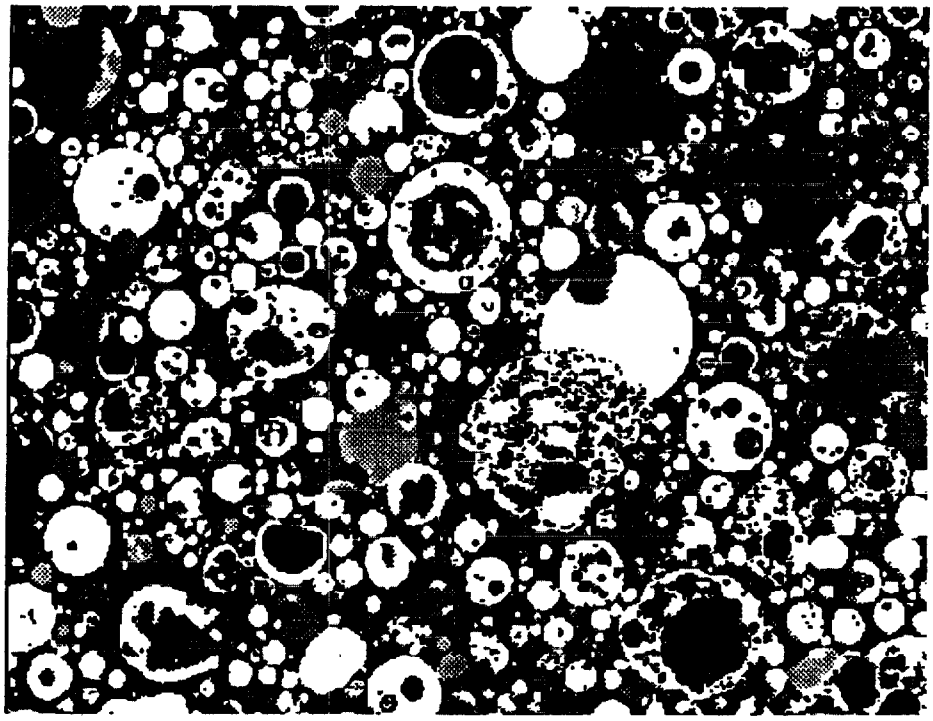

Figure 4: Final processed 2-D SEM/X-ray images for a class F fly ash. Image is 256 μm by 200 μm. Greylevels from brightest to darkest correspond to the following phases: aluminosilicate, calcium alumino-disilicate, anhydrite, inert, silica, and C_3A.

3.2 Analysis of cement ground to different finenesses

A set of clinkers ground to Blaine finenesses [10] ranging from about 200 m^2/kg to 650 m^2/kg have also been analyzed using the SEM/X-ray techniques. The same clinker was analyzed using optical microscopy to estimate its phase composition. Figure 6 provides final processed images for two of the grinding levels. One can clearly observe the differences in grain size and phase distributions present in the two images. As the cement is ground more finely, additional surface area is exposed, so that the surface area to volume ratio of the cements increases. This is illustrated quantitatively in Figure 7 which shows that the SEM measured fineness (surface area to volume ratio) correlates well with the measured Blaine fineness.

In Table I, the quantitative phase analysis results from the final segmented 2-D SEM/X-ray images are compared to one another and to the phase fractions estimated using optical microscopy point counting on the raw clinker. In general, the agreement between the different cement powder images and the raw clinker image is quite reasonable. The volume fractions of the C_4AF phase are slightly greater in the SEM images than in the clinker analysis, perhaps illustrating that an accurate determination of the ferrite phase via conventional optical microscopy is somewhat difficult, perhaps due to its small grain size. When comparing the results for the different finenesses, there are not any significant differences between the surface area phase fractions (relative to the corresponding volume fractions) to indicate that one particular phase is being preferentially exposed by the grinding. In general, the surface area fractions for the C_3A are higher than its corresponding volume fractions, and vice versa for the C_3S. This indicates that the cement particle surfaces are enriched in C_3A and deficient

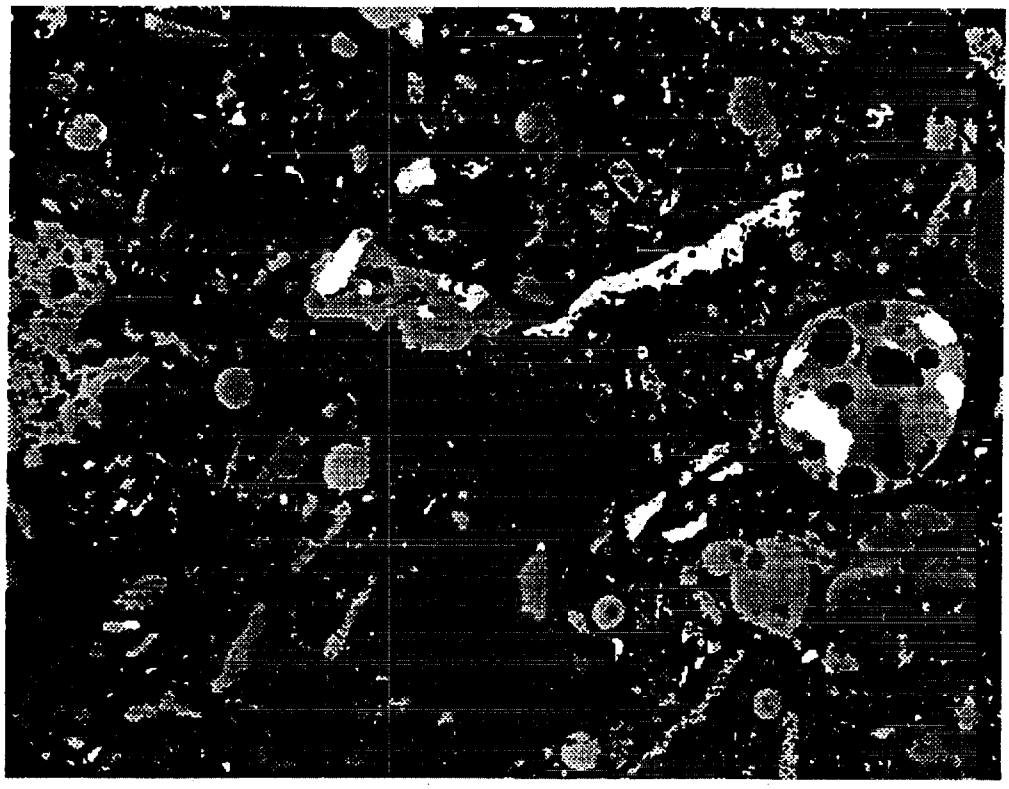

Figure 5: Final processed 2-D SEM/X-ray images for a municipal waste fly ash. Image is 512 μm by 400 μm. Greylevels from brightest to darkest correspond to the following phases: aluminosilicate, calcium alumino-disilicate, anhydrite, inert, silica, and calcium chloride.

in C_3S relative to the cement's bulk composition. This is at least partially due to the fact that the C_3S tends to be located in the larger particles, which have a reduced surface area to volume ratio relative to the smaller particles often containing the C_3A phase.

One important application for the images and the quantitative phase analysis results presented in this paper is to provide input for cement hydration and microstructural development models [11, 12]. Based on the quantitative phase fractions and the two-point correlation functions measured for the phases, a 3-D cement particle image can be reconstructed which matches the phase volume fractions, phase surface area fractions, and correlation structure of any cement of interest [8]. It is only after the starting cement powder is adequately characterized that accurate modelling of the hydration behavior and physical properties of cement-based materials is possible [13].

4 Conclusions

Techniques have been developed for analyzing a series of SEM and X-ray images of a cementitious material to quantitatively characterize its microstructure. For both fly ashes and cement powders, decision trees have been presented for determining the mineralogical phase to assign to each pixel comprising the two-dimensional image. Processed images are

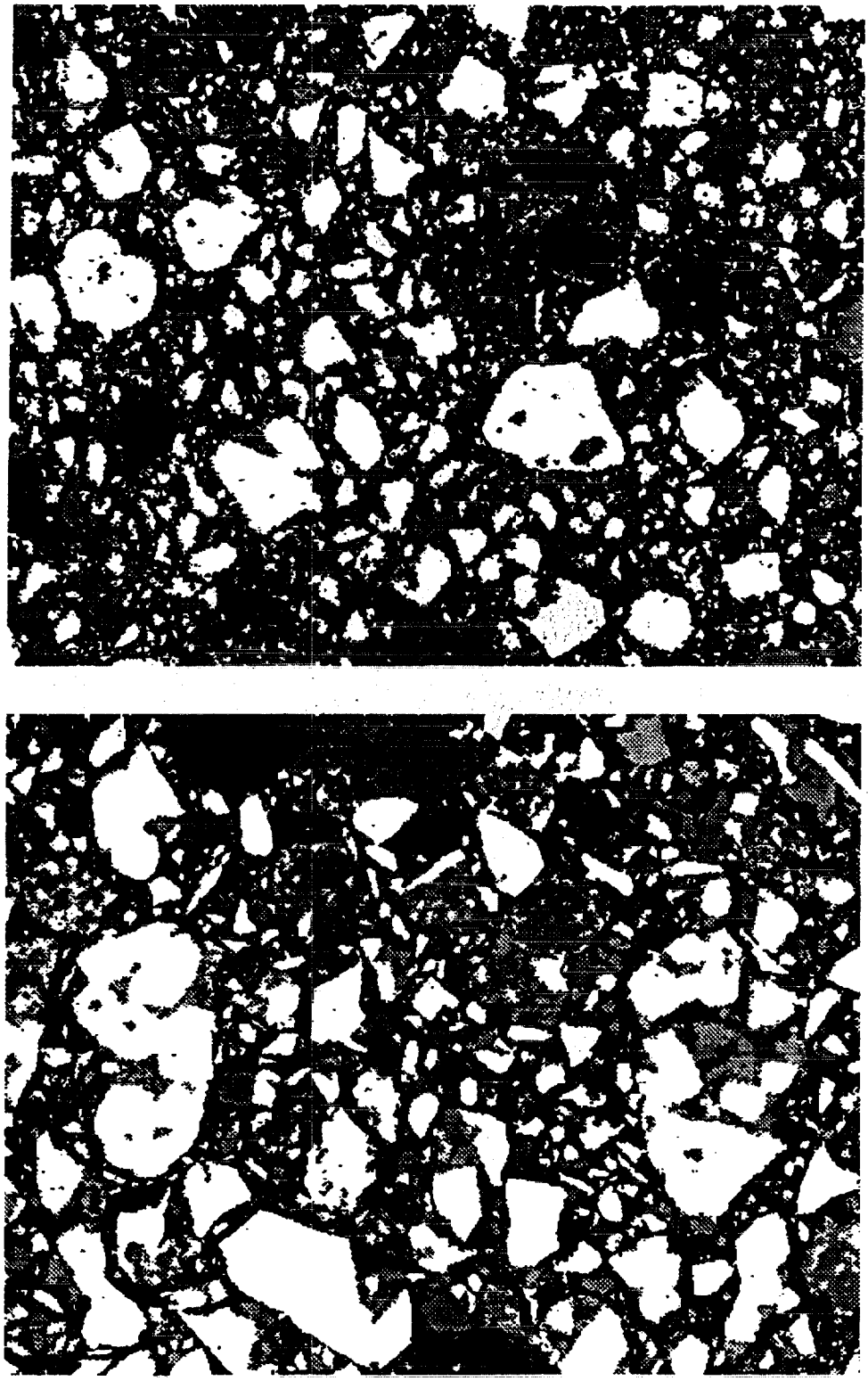

Figure 6: Final processed 2-D SEM/X-ray images for a portland cement ground to different fineness: top- 540.7 m^2/kg, and bottom- 197.0 m^2/kg. Each image is 256 μm by 200 μm. Greylevels from brightest to darkest correspond to the following phases: C_3S, free lime, C_4AF, calcium sulfates, C_2S, K_2SO_4, and C_3A.

Table 1: Volume fraction and surface area fraction for portland cement ground to different finenesses

Phase	Clinker	Cement powder Blaine fineness (m^2/kg) 654.0	540.7	370.0	279.0	197.0
	Volume fractions					
C_3S	0.740	0.770	0.752	0.746	0.643	0.763
C_2S	0.163	0.142	0.134	0.130	0.212	0.089
C_3A	0.076	0.045	0.077	0.084	0.077	0.083
C_4AF	0.022	0.043	0.037	0.041	0.068	0.065
		Surface area fractions				
C_3S		0.713	0.712	0.692	0.599	0.713
C_2S		0.176	0.131	0.122	0.233	0.098
C_3A		0.061	0.110	0.123	0.098	0.116
C_4AF		0.050	0.048	0.064	0.070	0.073

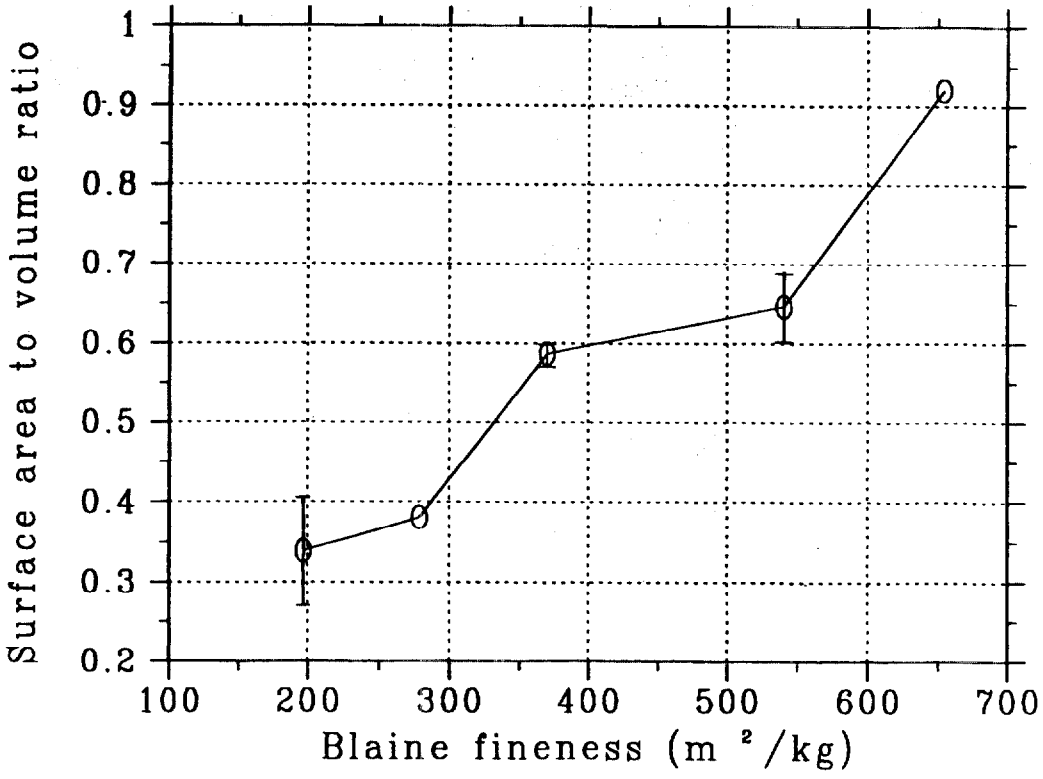

Figure 7: Image analysis surface area to volume ratio for four major clinker phases vs. measured Blaine fineness for a portland cement ground to five different finenesses. Error bars indicate one standard deviation for cases where two images were analyzed at a given fineness

conveniently analyzed to estimate phase volume fractions, phase surface area fractions, and phase two-point correlation functions. The quantitative data provided by these techniques is of paramount importance, both for materials characterization and for use as input into computer-based microstructural models of these complex materials.

5 Acknowledgements

The authors would like to thank Ms. Amanda Grasso of the Building and Fire Research Laboratory for preparing the cement specimens for the SEM analysis and the Partnership for High Performance Concrete Technology program (NIST) for funding this research.

6 References

1 Bentz, D.P., Quenard, D.A., Baroghel-Bouny, V., Garboczi, E.J., and Jennings, H.M., Modelling drying shrinkage of cement paste and mortar: part I. structural models from nanometres to millimetres. *Mater. Struct.*, Vol. 28, 450-458, 1995.

2 Taylor, H.F.W., Cement Chemistry (Thomas Telford, London, 1997).

3 Stutzman, P.E., Cement clinker characterization by scanning electron microscopy. *Cem. Concr. Aggregates*, Vol. 13 No. 2, 109-114, 1991.

4 Bentz, D.P., and Stutzman, P.E., SEM analysis and computer modelling of hydration of portland cement particles. in Petrography of Cementitious Materials Ed. S.M. DeHayes and D. Stark (American Society for Testing and Materials, Philadelphia, 1994) pp. 60-73.

5 Scrivener, K.L., The microstructure of anhydrous cement and its effect on hydration. *Proc. Mat. Res. Soc. Symp.*, Vol. 85, 39-46, 1987.

6 Scrivener, K.L., and Pratt, P.L., The microstructure of concrete. in Materials Science of Concrete I Ed. J.P. Skalny (American Ceramic Society, Westerville, OH, 1987) pp. 127-161.

7 Castleman, K.R., Digital Image Processing (Prentice-Hall, Englewood Cliffs, NJ, 1979).

8 Bentz, D.P., Three-dimensional computer simulation of portland cement hydration and microstructure development. *J. American Ceram. Soc.*, Vol. 80, No. 1, 3-21, 1997.

9 Bentz, D.P., and Remond, S., Incorporation of fly ash into a 3-D cement hydration microstructure model. NISTIR **6050**, U.S. Department of Commerce, August 1997.

10 ASTM **C 204** - Test Method for Fineness of Hydraulic Cement by Air Permeability Apparatus. Annual Book of ASTM Standards, Vol. 04.01, Cement; Lime; Gypsum. (ASTM, West Conshohocken, PA) 1998.

11 Bentz, D.P., and Haecker, C.J., An argument for using coarse cements in high performance concrete. *Cem. Concr. Res.*, Vol. 29, 1999.

12 Bentz, D.P., Garboczi, E.J., Haecker, C.J., and Jensen, O.M. Effects of cement particle size distribution on performance properties of cement-based materials, submitted to *Cem. Concr. Res.*, 1999.

13 Bentz, D.P., Modelling of cement microstructure: pixels, particles, and property prediction. *Mater. Struct.*, Vol. 32 (217), 1999.